Dual Cherenkov and Scintillation Response to High-Energy Electrons of Rare-Earth Doped Silica Fibers

Francesca Cova,[1] Marco T. Lucchini,[2,3,*] Kristof Pauwels,[4,3,†] Etiennette Auffray,[3] Norberto Chiodini,[1] Mauro Fasoli,[1] and Anna Vedda[1]

[1] *Department of Materials Science, University of Milano - Bicocca, Via Cozzi 55, 20125 Milano (Italy)*
[2] *Princeton University, Princeton, New-Jersey, 08544 (USA)*
[3] *CERN, Dept. EP-CMX, CH-1211 Geneva 23 (Switzerland)*
[4] *Department of Physics, University of Milano - Bicocca, Piazza della Scienza 3, 20125 Milano (Italy)*

(Dated: January 9, 2019)

The investigation of the characteristic luminescent response of Ce-doped silica fibers under exposure to electrons in the 20 - 200 GeV energy range is reported in this work, in order to explore the feasibility to employ silica-based fibers for a simultaneous dual-readout approach. The sol-gel method allows to prepare either doped or undoped fibers with high aspect-ratio and good purity, providing good flexibility and spatial resolution for the realization of a dual-readout detector. The dual Cherenkov and scintillation light emitted by silica-based fibers potentially offers applications in high-energy physics calorimetry as well as in other different fields, like radiation monitoring in medicine, security, and industrial controls. The response of the fibers, embedded in a tungsten-copper absorber block to obtain a Spaghetti-like geometry in a high-energy physics environment, has been investigated through a test beam campaign at the CERN Super Proton Synchrotron (SPS) facility. The discrimination of Cherenkov and scintillation light is demonstrated and discussed, along with a detailed investigation of the scintillation properties of the material: time-resolved spectroscopy, relative light output, and attenuation length are evaluated. The results presented in this study can pave the way for further material engineering and future applications.

PACS numbers: 29.40.-n, 42.81.-i, 78.47.+p, 78.70.-g
Keywords: Scintillating fibers; Cherenkov light; Dual-readout calorimetry; Sol-gel silica fibers

I. INTRODUCTION

Current and future ionizing radiation detectors need novel materials and concepts to improve and optimize their performances. The idea of fiber-shaped scintillation sensors has recently been developed: their application perspectives include devices for real-time dosimetry in medical systems [1], for beam monitoring and tracking [2], as well as high-granularity calorimeters for high-energy physics (HEP) experiments [3–6]. Based on the possibility of growing a great variety of fiber shapes and lengths, several calorimeter designs have been proposed [7], exploiting the flexibility of fibers to adapt for various needs. Indeed, fibers could be applied either as wavelength shifters for the collection and transport of light [8], or as scintillators and Cherenkov radiators in sampling and dual-readout calorimeters. In fact, fiber technology can allow a cost-effective implementation of the dual-readout approach to HEP measurements. Moreover, fibers enable the design of detectors with high spatial resolution, good timing properties, and radiation tolerance, which are essential requirements for future calorimeters [9].

The dual-readout calorimetry has been proposed as a technique to determine the electromagnetic shower fraction for individual events, by comparing on an event-by-event basis the signals generated in the form of Cherenkov and scintillation light [10]. It has recently been considered to improve the performance of hadronic calorimeters at future collider experiments (i.e. for the forthcoming High Luminosity Phase of the Large Hadron Collider at CERN) [11]. In fact, scintillation light is proportional to the total energy deposited by the electromagnetic shower particles, while Cherenkov light is produced only by charged, relativistic particles which are almost exclusively found in the electromagnetic shower component. Several approaches were suggested for the dual-readout concept: amongst them, either the use of two independent active media or the *a posteriori* decomposition of scintillation and Cherenkov components of the light emitted by a single material [12, 13].

Besides HEP experiments, the dual-readout is involved also in several other fields. Indeed, dual Cherenkov and scintillation readout has also been proposed for calibrating and monitoring high-energy electron beam profiles in radiotherapy and for the optical imaging of ionizing radiation in the clinical field [14, 15]; in addition, its use can be employed for applications in security, industrial X-ray imaging and radiography [16, 17]. Furthermore, the dual-readout can be exploited to probe the transport of solar energetic particles, allowing to cover the energy range from tens to hundreds of MeV with a single detector, as reported in [18].

The research on fibers based on inorganic crystalline scintillators has seen a significant development in the

* Corresponding author: marco.toliman.lucchini@cern.ch
† Currently at ESRF, The European Synchrotron, 71 Avenue des Martyrs, Grenoble (France)

recent years, and their use with rare earth (RE) ions as luminescent activators for high-energy radiation detection has already been intensively studied: $Y_3Al_5O_{12}$ (YAG):Ce single crystal fibers [19, 20] and $Lu_3Al_5O_{12}$:Ce fibers grown by micro-pulling down technique [21, 22] have been characterized with beam tests and under high levels of γ and proton irradiation.

Moreover, it has been pointed out that scintillators based on glass matrices could be a good alternative to heavy crystals, because of their simpler preparation procedure, better shaping possibilities, faster pulling rates, and their lower costs of production [23–26]. The sol-gel technique was proven to allow a good control, at a relatively low densification temperature, of RE ions incorporation and of their dispersion inside the glass matrix [27, 28]: the glass synthesis can be performed by using high purity precursors, reducing the level of unwanted impurities, which is an essential feature for the radiation hardness of such materials. Several studies were devoted to the realization of RE-doped silica glasses prepared by sol-gel route for HEP applications [29, 30]. Previous results proved that sol-gel silica-based fibers can be considered a good scintillator material with a suitable attenuation length: however, their radiation hardness has still to be optimized for applications in HEP experiments with very high levels of radiation [31].

In this work, we present an in-depth investigation of the possibility and the potentiality to employ RE-doped silica fibers for the simultaneous Cherenkov and scintillation dual-readout approach. They are proposed as the active material in a Spaghetti-like electromagnetic calorimeter prototype (SpaCal in the following); their scintillation properties, as the results of a test with electrons beam in the energy range of 20 - 200 GeV performed at the H4 beam line of the CERN SPS North Area facility, are also reported within the scope of this study.

II. EXPERIMENTAL SETUP AND PROCEDURE

A. Sol-gel silica fibers and SpaCal module

Ce-doped silica glasses were prepared by the sol-gel method using tetramethylorthosilicate (TMOS) and Ce(III) nitrate as precursors. Alcogels were formed after gelation and subsequently dried in a thermostatic chamber for a few weeks. The obtained xerogels were densified at 1225 ℃ in oxidizing (O_2) atmosphere to produce Ce-doped preforms. Cylindrical fibers were then drawn with a fluorinated SiO_2 cladding wrapping the RE-doped core, in order to guarantee the light guiding by the core-cladding interface: the core diameter is 0.60 mm and the total fiber diameter is 0.75 mm. The numerical aperture of these fibers is estimated to be ~ 0.17. Fibers were left uncoated and cut into 200 mm long pieces.

A tungsten-copper (W-Cu, 75%-25%) absorber block of total dimensions 60 x 60 x 200 mm^3 made of square 1.1 x 1.1 mm^2 holes, 1.8 mm apart, was filled with fibers to obtain a sampling SpaCal prototype, shown in Fig. 1(b), in which the fibers are used as the active scintillating material. These dimensions and fiber packing were optimized according to practical constrains.
Five distinct channels of fibers in the SpaCal module are sketched in Fig. 1(a) and filled with 80 fibers each, for a total bundle diameter of approximately 15 mm: fibers were YAG:Ce (central channel), 0.002% Ce-doped silica (top left), plastic Kuraray SCSF-3HF used as reference (top right), 0.05% and 0.0125% Ce-doped silica (bottom left and right respectively).

In this work, we decided to focus the investigation on the response of Ce-doped silica fibers with the highest concentration compared to that of plastic fibers.

A set of 6 Hamamatsu Photonics R5380 photomultiplier tubes (PMT) with bialkali photocathodes and borosilicate glass windows of 20 mm diameter were used to read out the light from the fibers in the SpaCal module: top channels were read out only from the rear side, bottom channels from both sides of the fibers, to exploit the use and the advantages of the double side readout technique [21, 31]. Silicon rubber optical interface (EJ-560, Eljen Technology) with refractive index of 1.43 was used to couple the fibers and the PMT window, in order to improve light extraction.

The module was mounted inside a light tight aluminum box providing optical and thermal insulation, with a water cooled system to maintain a constant temperature of 18 $\pm$ 0.5 °C: the box was installed on a remotely-controlled horizontal - vertical (x - y) table with a displacement range of $\pm$ 300 mm and positioning accuracy of $\sim$ 1 mm. The frame of reference used throughout this paper has the x-axis horizontal on the experimental table, the y-axis pointing vertically upwards, and the z-axis aligned and pointing in the same direction of the beam line.
The module was exposed to the beam in two different configurations, described in Fig. 1(c), hereafter referred to as *pointing* and *transverse*. In the former case, the beam was aligned with the fibers; the secondary particles, produced during the primary interaction of the high-energy electrons impacting on the absorber and denoted as *shower*, developed all along the fiber length, while laterally extending inside the fiber bundle. In fact, the transverse dimension containing on average 90% of the shower's energy deposition (*Molière radius*, [32]) is estimated to be $\sim$ 17 mm. In this configuration, the analysis of the time decay of the emitted light intensity (denoted as pulse shape) and the study of the fibers response as a function of the varying incident beam energy were performed. In the transverse configuration, the beam was impinging at cross angle with respect to the fibers, in order to carry out an analysis of the attenuation profiles through a position scan, moving the table by discrete steps of $\sim$ 30 mm.

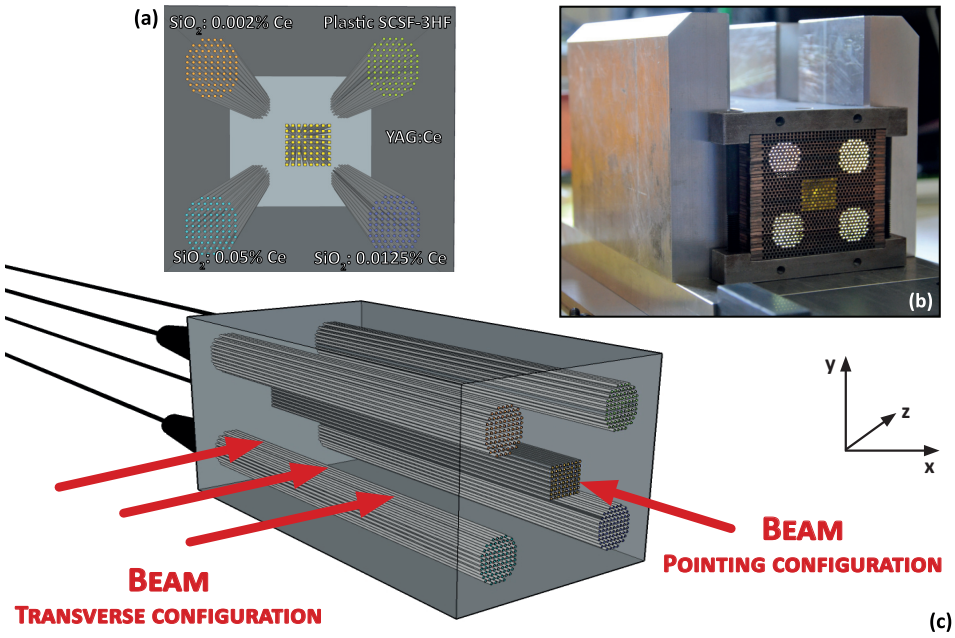

FIG. 1. SpaCal setup. (a) Schematics front view of the SpaCal prototype: the labels describe the type of fibers in each channel. (b) Picture of the SpaCal prototype made of 5 channels with 80 fibers each in a tungsten-copper absorber. (c) Schematics side view of the SpaCal module, showing pointing and transverse configurations.

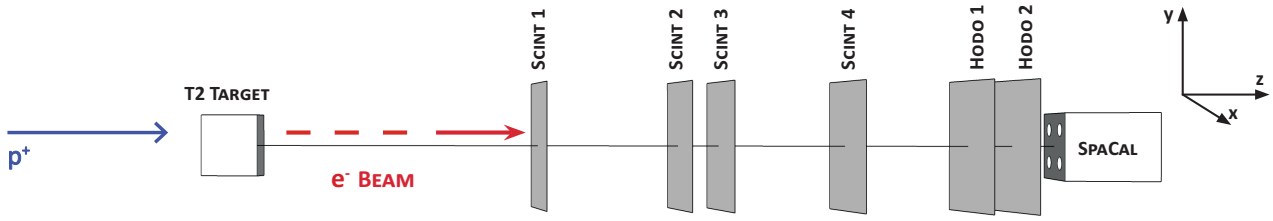

FIG. 2. Sketch of the last stage of the H4 beam line at CERN, SPS. The SpaCal prototype, the scintillation counters, and the hodoscopes used in this analysis are shown. The blue arrow displays the primary proton beam impacting on the target; the red arrow indicates the electron beam direction.

B. Beam line

The experiments were performed at the H4 beam line of the CERN SPS North Area facility, which provides electron beams in the 20 GeV to 200 GeV range with hadron and muon contamination below 0.2%. Primary protons injected into the SPS interact with the T2 beryllium target to generate secondary particles including electrons and pions. The type and energy of the particles is selected after the target by a set of magnets and collimators. The incoming electrons are detected by a set of four plastic scintillation counters used to trigger the data acquisition system. The beam is composed by subsequent electron packets lasting 4 s and separated by around 30 s. Each packet contains approximately 10^4 electrons, among which $\sim 10^3$ are useful for the measurements exploiting the coincidence with plastic scintillation counters. The impact point of the beam particles on the module was accurately measured using two sets of beam hodoscopes, shown in Fig. 2. Each set comprised two orthogonal planes of 64 scintillating fibers with square cross-section 0.5 x 0.5 mm^2, read out by a multianode PMT. Each plane provides, respectively, a measurement of the electron position in the x and y directions with a nominal precision better than 200 μm [33].

C. Experimental procedure

The coincidence of signals from the beam counters has been used to generate the trigger for the event acquisition, while the hodoscopes allowed to reconstruct the impact point of the electrons on the SpaCal. The signals from the PMTs were digitized by a CAEN V1742 module operated at a sampling speed of 2.5 GHz and providing a time gate for the recorded pulses of 350 ns.

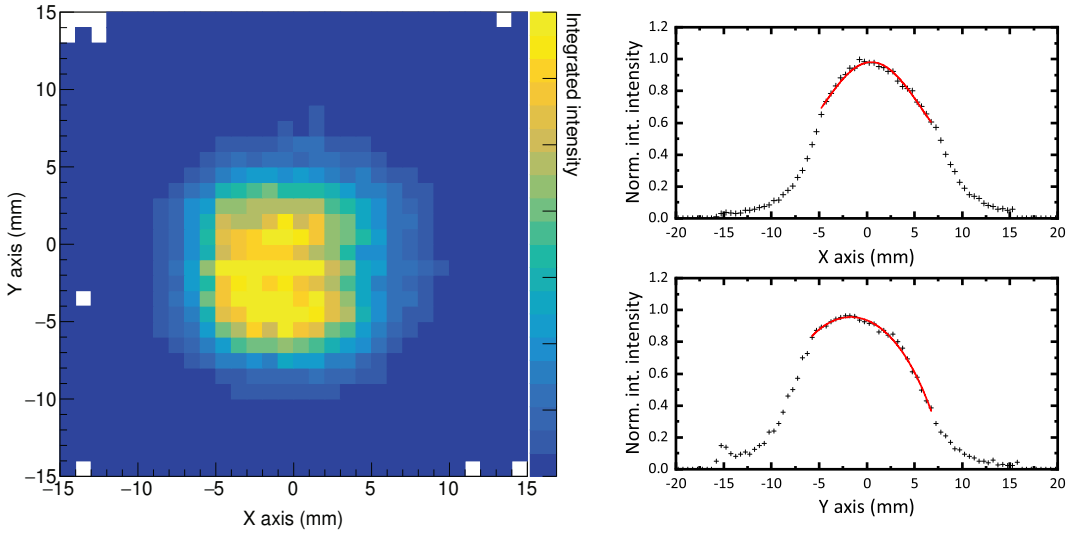

FIG. 3. Left: contour plot of the fibers average integrated intensity as a function of the impact point along x- and y-axes for 150 GeV electrons beam with the module in pointing configuration. A beam spot selection of 20 mm^2 is considered for the analysis. Right: projections of the average integrated intensity of a fiber channel as a function of the impact point along x-axis (top panel) and y-axis (bottom panel). Red lines: polynomial symmetric fit function $A \cdot (x - x_0)^4 + B \cdot (x - x_0)^2 + C$ used to determine the channel center.

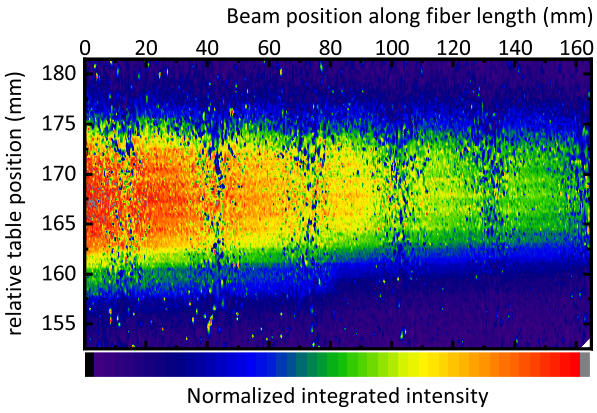

FIG. 4. Fibers signal in transverse configuration as a function of beam position moving from left to right, as detected by the left photodetector. On the z-axis, the integrated intensity normalized to the maximum reported from 0 to 1 in linear scale is displayed. The vertical blue stripes are due to the small number of events at the edges of the beam profile when changing discretely by steps the table position with respect to the beam.

The response of a particular channel varies with the impact point, due to the variation of the shower containment and the consequent change of the energy deposited within the active volume: the center of each channel was defined as the position where the maximum response was observed and this maximum was obtained by a fit to the measured response profiles using a 4^{th}-order polynomial, as illustrated in the right panels of Fig. 3. This procedure allowed the module to be correctly centered on the beam. The left panel shows a plot of the beam profile in pointing configuration as detected by the rear PMT of the Ce-doped fibers channel. A beam spot selection of 2.5 mm radius from the center of the bundle, corresponding to a 20 mm^2 area, was applied to limit shower transverse leakage.

After the position of each channel was determined, the high voltage supplied to each PMT was adjusted to have the highest signal without saturation: it was set to 1700 V for Ce-doped silica fibers and 800 V for plastic fibers. This setting allowed the use of the same PMT gain for the whole energy scan in the 20 - 200 GeV range.

Energy scans were performed with the beam incident on the center of each fibers bundle for 20, 50, 100, 150 and 200 GeV electrons.

As a last step, the whole box containing the module was rotated by 90 degrees clockwise in order to have the beam impacting on the lateral side of the fibers, allowing measurements of the attenuation length. A contour profile of the signal from Ce-doped silica fibers in this latter configuration is shown in Fig. 4, as detected by the left PMT: it is the superposition of six different measurements obtained by shifting the detector in steps of 30 mm to allow the reconstruction of the attenuation profiles, further discussed in Section III D.

Before comparing the signals from different channels, the photodetectors have been intercalibrated in laboratory. The intercalibration coefficients account for channel-by-channel response variations, due to the photocathode quantum efficiency and fibers-to-PMT optical coupling, and variations mostly related to the different

high voltage applied to fit within the analog-to-digital converter (ADC) dynamic range and thus different amplification gain.

In order to estimate the amount of light produced in each fibers bundle, an absolute calibration of the photodetector response was also performed. A $Lu_{2(1-x)}Y_{2x}SiO_5$:Ce crystal of 1 mm^3 was used as reference and measured under exposure to a ^{137}Cs γ source with each PMT used in the test beam experiment: the reconstructed distribution was compared to that of a calibrated PMT to get the ADC-to-photoelectrons conversion factors.

III. TEST BEAM RESULTS AND DISCUSSION

The test beam experiment and the following analysis provide a thorough investigation of the scintillation properties of Ce-doped sol-gel silica fibers under high-energy electromagnetic particles. The response of these fibers to high-energy electrons has been studied for the first time with the SpaCal calorimetric module in both pointing and transverse configuration, thus allowing for an evaluation of scintillation decay time, light output, and attenuation length.

The discussion will focus at first on the pulse shape analysis, and then on the reconstruction of the shower profile and energy. A method for Cherenkov and scintillation light discrimination is proposed to carry out a separate analysis of the two components of the emitted light, strengthening the possibility of Ce-doped silica fibers applications for simultaneous dual-readout.

A. Pulse shape analysis

The waveforms from the different types of fibers in the SpaCal module are recorded in a 350 ns time interval and reported in the top panel of Fig. 5: they were calculated by averaging over the selected events for 150 GeV electrons having their impact point within 2.5 mm radius from the center of a given channel, as described in Section II C.

SiO_2:0.002%Ce doped fibers did not show any scintillation light, probably too weak to be detected, and no analysis was carried out on their luminescence decay.

In the following, the attention has thus focused on the comparison between SiO_2:0.05% Ce and plastic fibers decays, which have been fitted by the sum of exponential contributions. Plastic fibers scintillation decay is characterized by a single component with decay time $\tau = 9 \pm 1$ ns, whereas Ce-doped silica fibers feature two contributions with $\tau_1 = 55 \pm 5$ ns and $\tau_2 = 145 \pm 22$ ns and fractional weights $26 \pm 3\%$ and $74 \pm 3\%$ respectively. The possible presence of a third faster component cannot be inferred by this analysis, because the first part of the decay is strongly influenced by the fast Cherenkov emission. In the bottom panel of Fig. 5, the evolution of

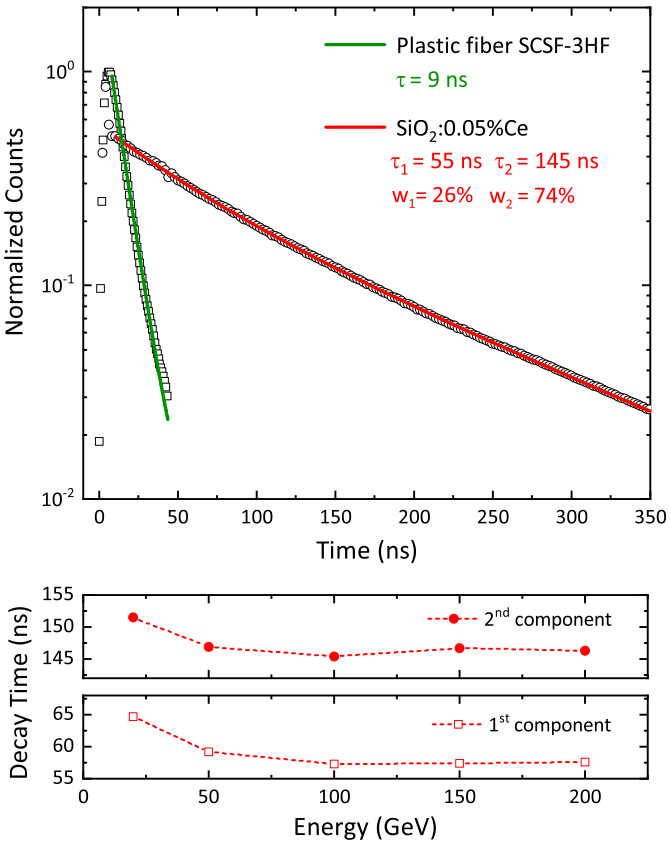

FIG. 5. Top panel: normalized average pulse shape of Ce-doped silica and plastic fibers (dotted lines) and fit of the scintillation decay (solid lines) with a sum of exponential contributions for 150 GeV electrons beam. In the legend, decay time and weight for each component is reported. Bottom panels: decay time for the two components of Ce-doped silica fibers scintillation decay is displayed as a function of the incident energy. Lines are guides for the eye.

the decay time for the two components of Ce scintillation decay is reported as a function of incident beam energy: an overall slower scintillation decay time at the lowest energies can be observed for both the components. We suggest that this effect can be ascribed, from a general point of view, to a variation of the excitation density in the material with decreasing incident energy, which consequently leads to differences in the scintillation recombination kinetics [34]. This phenomenon will be the subject of further investigation, in order to deeply characterize and compare the scintillation kinetics of Ce-doped sol-gel silica fibers under various ionizing radiation sources with different distributions of excitation density in the material.

The decay times of Ce-doped fused silica fibers produced by dissolving the dopant in the glass matrix were reported by Akchurin et al. [26] and were evaluated to be 20.8 ± 5.4 ns and 93.0 ± 12.6 ns for τ_1 and τ_2 respectively in a 200 ns time window, but with similar fractional

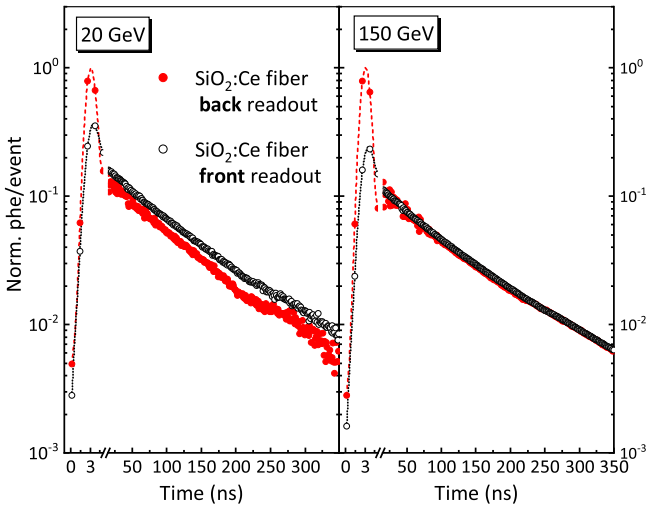

FIG. 6. Average pulse shape normalized to the number of events for SiO_2:Ce fibers for 20 GeV (left panel) and 150 GeV (right panel) electrons beam. Back and front readout are compared. Dashed lines are guides for the eyes.

weights. The faster decay times, compared to those obtained in this study, can be ascribed to a different incorporation of Ce ions in the silica-based matrix, studied in [26], containing a significant percentage of additional dopant ions, especially Al.

B. Cherenkov and scintillation light discrimination for Ce-doped silica fibers

In Fig. 6 the average pulse shape of Ce-doped silica fibers is displayed as recorded by the back (red) and front (black) PMT and normalized to the maximum of the back signal. The prompt emission, enlarged in the first part of the decay, can be ascribed to the Cherenkov effect [5, 35–37], occurring in both the RE-doped core and the fluorinated cladding of glass fibers; the convolution with the scintillation emission has to be taken into account and, in the following, a detailed analysis is carried out to distinguish the two contributions.
Cherenkov light is emitted in the forward direction at a characteristic angle with respect to the track of the charged particle. Thus, Cherenkov signal is expected to be higher in the rear detector, confirmed by the amplitude of the peak in the first part of the waveform.
On the other hand, scintillation emission is isotropic, and the same amount of scintillation light is expected in both rear and front detectors, as observed in the case of 150 GeV incident electrons (right panel). This occurs when the shower maximum falls approximately in the center of the fiber length, so that attenuation effects are the same for light traveling in the two directions. For the lowest energy of 20 GeV (Fig. 6 left panel), the scintillation light in the front PMT is more intense than in the rear one, thus proving the dependence of the position of the maximum of the shower L_{max} on the incident beam energy, described by Eq. 1 [38], where $X_0 = 0.8$ cm is the radiation length [32] of the calorimeter prototype evaluated by Geant4 numerical simulation.

$$L_{max} = X_0 \, (4.2 + 1.8 \cdot \ln E) \tag{1}$$

The average position of the shower maximum shifts towards the back of the absorber with the increase of the energy of incoming electrons: this change in the behavior of the shower profile along the longitudinal axis is expected to produce a different ratio R_{fb} of the front (S_{front}) over back (S_{back}) signals measured at the two opposite ends of the fibers, defined in Eq. 2.

$$R_{fb} = \frac{S_{front}}{S_{back}} \tag{2}$$

In the top panels of Fig. 7, the value of R_{fb} is plotted against the position of the maximum of the shower (L_{max}) in cm, in a semi-logarithmic scale. The average ratio R_{fb} of the front and rear signal decreases due to the shift of the shower maximum towards the rear side of the absorber block at high energies. It has been evaluated for both Cherenkov (left panel) and scintillation light (right panel) and a clear correlation with the beam energy can be observed and used for an estimation of the attenuation length of the fibers with the calorimetric module in pointing configuration, as discussed in [5]. The attenuation values so obtained are $L_{att,\ Ch} = 9 \pm 2$ cm and $L_{att,\ Scint} = 25 \pm 6$ cm for Cherenkov and scintillation emission respectively. The different nature of Cherenkov and scintillation light can account for the different correlations displayed in Fig. 7.
In the bottom panels, the ratio of the Cherenkov over scintillation signal as a function of beam energy is reported for the back (left) and front (right) readout, in order to evidence the different dependence of the two emissions on the shift of the shower maximum position towards the back of the module with increasing incident energy. Cherenkov light intensity increases in the back channel and decreases in the front channel faster than scintillation, with the shower maximum moving towards the back, thus suggesting a greater attenuation of UV Cherenkov photons. This result will be stressed in Section III D, where the attenuation length in transverse configuration is evaluated for both the emission contributions.

The separate study of Cherenkov and scintillation signals has been carried out through an event-by-event pulse shape analysis, by integrating the waveform of the single selected event in different time intervals, namely in the first 5 ns for Cherenkov emission, and in the remaining part for the scintillation contribution. This method leads to an underestimation of the scintillation component because it does not take into account the scintillation signal emitted in the range $0 < t < 5$ ns, and thus a reconstruction of the true scintillation integrated emission has

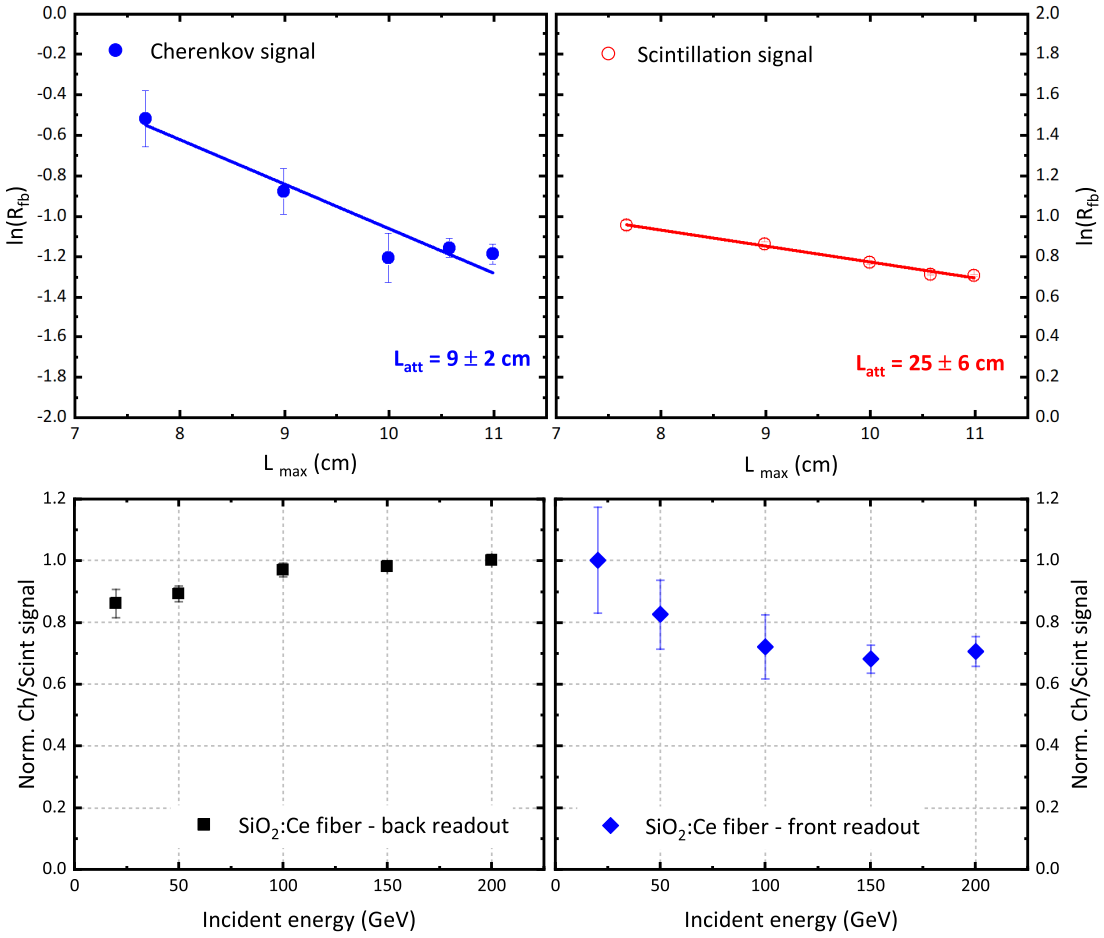

FIG. 7. Top panels: linear correlation between the natural logarithm of the ratio of back over front signal and the position of the shower maximum in cm, proportional to the natural logarithm of the incident energy according to Eq. 1, for Cherenkov (left) and scintillation light (right). Bottom panels: ratio of Cherenkov over scintillation signal as a function of the incident energy for back (left) and front (right) readout.

to be performed exploiting the fit procedure carried out on the average waveform of Fig. 5.

By defining S and C the integrated scintillation and Cherenkov emissions in the two separated time intervals calculated event by event, we can estimate the true integrated signals S_t and C_t by solving the set of Eqs. 3, where a is the ratio between scintillation integrated signal evaluated at $t > 5$ ns and the extrapolation to t = 0 ns of the area under the exponential decay fit curve of the average pulse shape displayed in Fig. 5.

$$\begin{aligned} S_t &= \frac{S}{a} \\ C_t &= C - S \cdot \left(\frac{1}{a} - 1\right) \end{aligned} \tag{3}$$

This method has been used to reconstruct the distributions of photoelectrons for both Cherenkov and scintillation emission for 150 GeV electrons beam, reported as an example in top panels of Fig. 8, where the ADC-to-photoelectrons coefficients have also been taken into account. A difference of 3-4% in the evaluated amount of scintillation signal between front and back readout can be observed in the top right panel of Fig. 8: it is comparable to the precision of the photodetectors calibration. A Gaussian fit has been performed on the reconstructed distributions in the 20 - 200 GeV energy range to estimate the peak positions. In the bottom panels of Fig. 8, the position of the peak, converted in photons and divided by the incident energy, is reported as a function of the incident energy itself: the light readout by the rear PMT shows a stronger non-proportionality with respect to the front readout. Such a behavior can be related to the displacement of the maximum of the shower as a function of the incident energy, combined, only for Cherenkov component, with the directionality of the emission. In any case it can be noticed that Cherenkov light contribution is only around 5% to 10% with respect to scintillation for all energies.

We can conclude that under exposure to high-energy particles beam probe, the two contributions of Cherenkov and scintillation light can be detected simultaneously

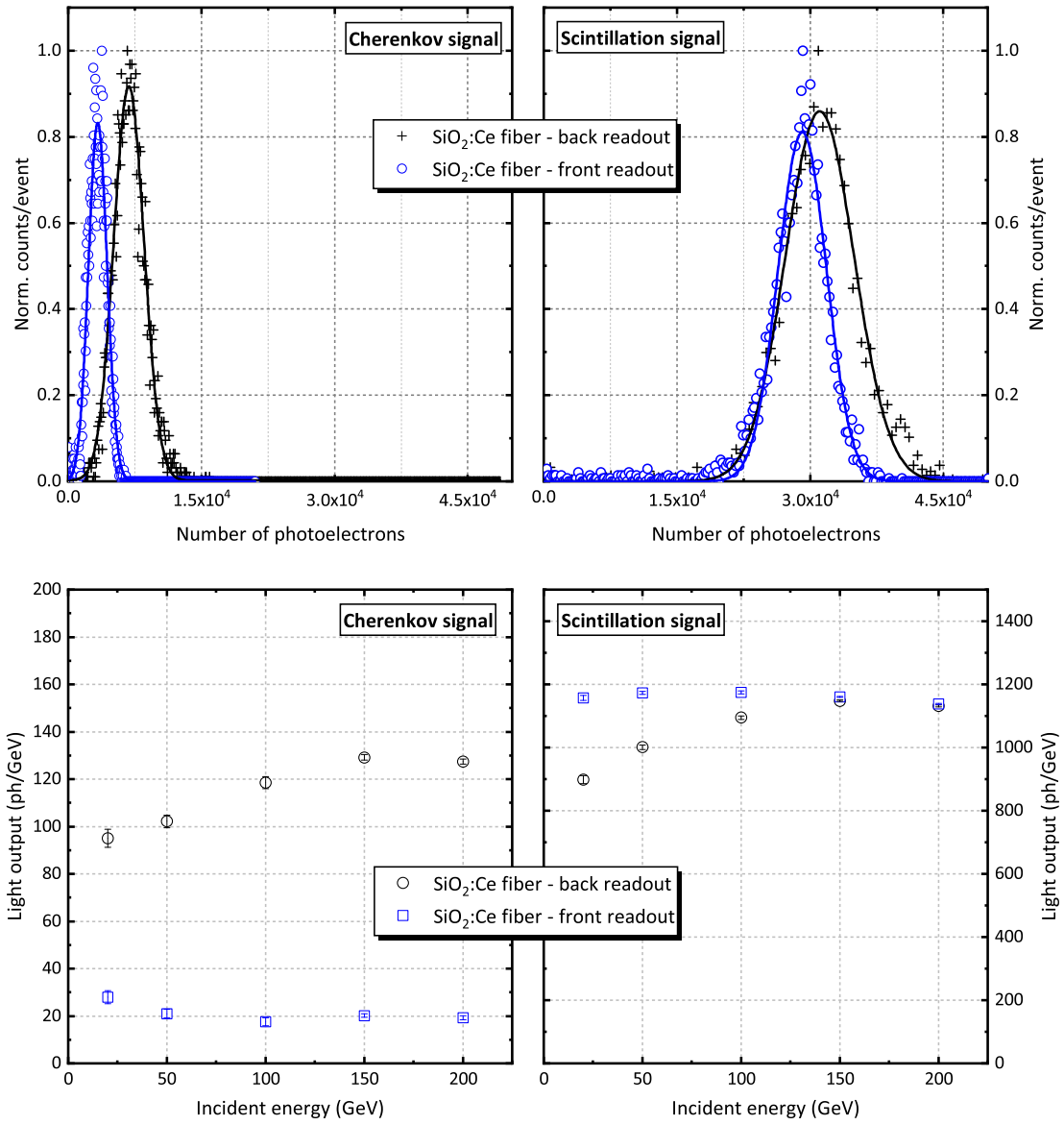

FIG. 8. Top panels: normalized distributions of photoelectrons for Cherenkov and scintillation signals for SiO_2:Ce doped fibers readout from both the ends under 150 GeV electrons beam. Bottom panels: correlation between light output of Cherenkov (left) and scintillation signal (right) and incident beam energy. The y-axis reports photons over GeV of incident energy which is not therefore an absolute scale of the light yield of the material. Error bars are within the size of data points.

with the same Ce-doped silica fibers bundle. A characteristic dual response of the fibers has been observed and the feasibility to carry out a well-distinguished analysis of the two components of the pulse shape has been demonstrated.

C. Energy reconstruction and linearity

The particle energy can be reconstructed by applying intercalibration coefficients, calculated as described in Section II C, and considering only events within a beam spot of 2.5 mm radius around the center of the fibers channel, in order to account only for electrons which develop the shower inside the fiber bundle. The total contribution has been summed up event by event to reconstruct the signal, taking into account the ADC-to-photoelectrons calibration factors. Obtained distributions of the reconstructed amplitude in the 20 - 200 GeV range are shown in the left panel of Fig. 9 for Ce-doped silica fibers and fitted with a Gaussian function to estimate the peak position and its width.

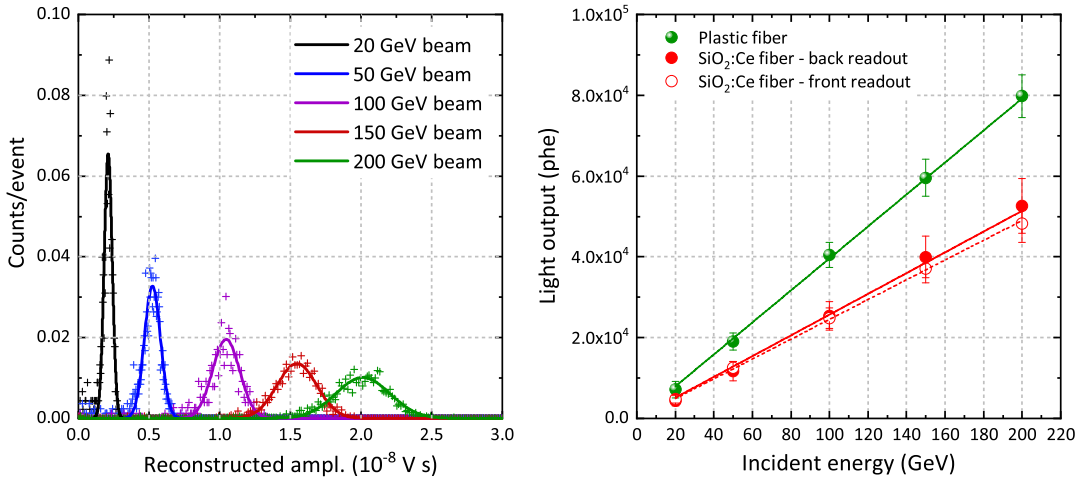

FIG. 9. Left panel: distributions of reconstructed amplitude at different beam energy. SiO_2:Ce doped fibers signal is reported. Right panel: linear correlation between peak values of reconstructed amplitude distributions and incident beam energy. The light output in photoelectrons is evaluated.

The peak positions of the reconstructed amplitude distributions have then been converted in number of photoelectrons and reported in the right panel of Fig. 9, where a good correlation with the incident beam energy can be observed. A comparison of the light output of the different types of fibers is reported in the right panel of Fig. 9, thus showing that plastic fibers are brighter than Ce-doped silica fibers by a factor 1.5. It should be taken into account that the density of the plastic fibers (1.2 g/cm^3) is lower than that of silica fibers (2.2 g/cm^3), and therefore the incident beam deposits a lower fraction of energy in the plastic fibers channel.
However, the higher density of silica fibers can be regarded as an advantage because it permits to devise calorimeters with a shorter Molière radius, compared to detectors using plastic fibers as the active component; the shower is thus confined in a more compact area.

The energy resolution $\frac{\sigma_E}{E}$ of the reconstructed amplitude was found to decrease with increasing incident energy, thus following the expected trend [39]: at 200 GeV it could be estimated to be around 15%, which mainly accounts for contributions from the partial transverse shower containment within a single fiber bundle and from the non-uniformity of the fibers themselves.

D. Attenuation length of Ce-doped silica fiber

A non-uniformity along the fiber length in the efficiency of the light extraction at the fiber ends, if not corrected for (e. g. by means of a double side readout [39]), can affect the response and the performance with high-energy particles. A characterization of the photoluminescence emission attenuation length of Ce-doped silica fibers had already been carried out previously using a 370 nm pulsed LED as excitation source: the experimental procedure and results are accurately described in [31].

The measurement has been repeated with 150 GeV electrons beam and the SpaCal module in transverse configuration, placing the table at 6 different x coordinates to obtain a nearly uniform scan of the entire length of the fibers. To enhance the signal, a beam spot selection of $\pm$ 2 mm along the y-axis has been applied for the computation of the energy deposit.
Exploiting the double side readout technique, the transverse profiles have been analyzed, parametrizing the curve with a single exponential decay according to Eq. 4: S_L and S_R are the signals detected by the left and right PMT respectively, d is the distance and L_{att} is the parameter for the characteristic attenuation length of the fiber to be calculated.

$$\frac{S_L}{S_R} = A_0 \cdot exp\left(-\frac{2d}{L_{att}}\right) \tag{4}$$

Normalized transverse profiles and their fit are reported in Fig. 10: both single fibers (left) and fibers bundle in the SpaCal module (right) have been measured, the former being readout with two UV-sensitive H6610 Hamamatsu Photonics PMTs, using two blocks of iron and lead as pre-shower.

The discrimination of Cherenkov and scintillation signals has been performed for the fibers in the SpaCal module, and the attenuation length values estimated with the fit procedure are $L_{att,\ Ch} = 12 \pm 3$ cm and $L_{att,\ Scint} = 23 \pm 6$ cm for Cherenkov and scintillation emission respectively. Cherenkov light was observed to have a shorter attenuation length, thus confirming results shown

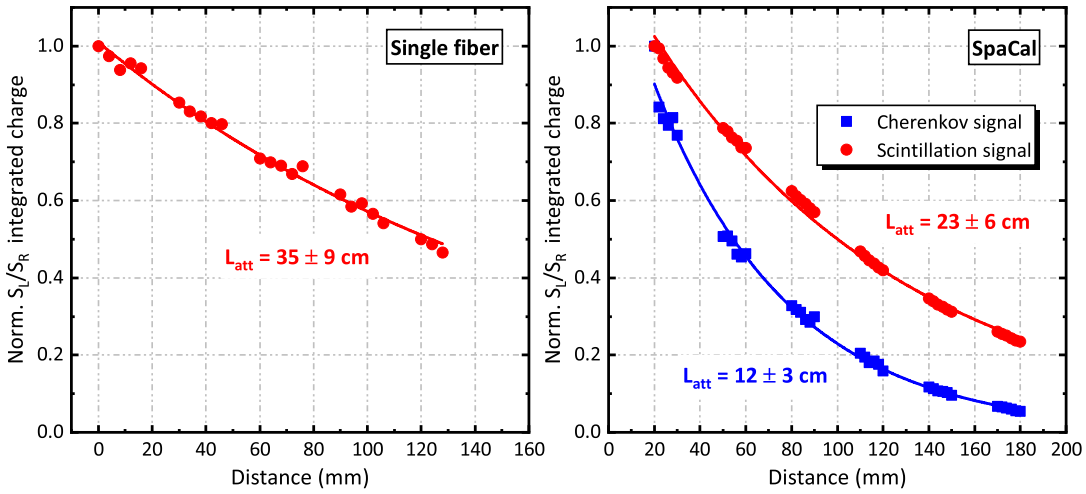

FIG. 10. Attenuation length curves for SiO_2:Ce doped fibers measured in transverse configuration under 150 GeV electrons beam and using the double side readout technique: on the y-axis, the ratio of left over right PMT signal is reported. Left: measurement of a single fiber with UV-sensitive PMTs. Right: attenuation measurement "in SpaCal" configuration. Discrimination between Cherenkov and scintillation signal is considered.

in Fig. 7 and described in Section III B: this could be ascribed to the fact that Cherenkov photons are mainly in the UV spectral region and have a higher probability therefore to be absorbed by Ce luminescent centers and by matrix defects.

For single fibers, only the analysis of the scintillation signal was possible, due to the presence of spurious signal from the PMT windows. Scintillation attenuation length was found to be worse in the SpaCal configuration with respect to single fibers ($L_{att,\ Scint}$ = 35 ± 9 cm): this could be related to the silica cladding in contact with the absorber, leading to a variation of the refractive index at the fiber boundary and to a loss in the total internal reflection efficiency, which causes an increase of the light leakage before reaching the photodetector.

A further optimization of the fiber cladding geometry and a proper quenching of the cladding light propagation modes are thus suggested by this analysis, in order to improve the light extraction through total internal reflection. Nevertheless, the attenuation profile measured in the beam test for the single Ce-doped silica fiber is in good agreement with laboratory measurements [31].

IV. CONCLUSIONS

Our results obtained under the exposure to high-energy electrons allowed a detailed investigation of the scintillation properties of Ce-doped sol-gel silica fibers embedded as the active component in a Spaghetti-like electromagnetic calorimeter prototype. The decay time of Ce^{3+} scintillation, silica fiber attenuation length, and relative light output were evaluated by testing the SpaCal module both in pointing and transverse configurations with respect to the incident beam. The scintillation time decay was analyzed and the reconstruction of the shower profile and energy were addressed.

The feasibility of a simultaneous dual-readout approach and the discrimination of Cherenkov and scintillation emitted light were demonstrated.This unique feature allows the realization of calorimeters made of a single type of fibers to read the dual emission, instead of two with either different doping or density.

The presented results support the potential applications and perspectives of silica fibers for dual-readout calorimetry, as well as for beam monitoring, radiotherapy in the medical field, security, and industrial X-ray imaging.

Further material engineering will look for the optimization of the fiber geometry, towards a complete quenching of the cladding propagation modes, to improve the light extraction from the fiber core together with the radiation hardness, in order to exploit the possibility that sol-gel silica offers to realize long either RE-doped or undoped silica fibers with good attenuation length in a cost-effective way.

ACKNOWLEDGMENTS

The authors would like to sincerely thank Andrea Polesel, Rosalinde Pots, Nazar Bartosik, Alessandra Cappati, and Muhammad Bilal Kiani for taking part in the test beam campaign and for all the time and work they put into it. The authors are grateful also to Hubert Gerwig and Nicolas Siegrist from CERN EP_CMX for the realization of the SpaCal absorber.

This work has been carried out in the frame of the Crystal Clear collaboration and supported by H2020

Rise Intelum Project (644260), H2020 Research Infrastructures (AIDA2020) (654168), ASCIMAT Project (690599), and EIT SPARK Project (16290).

[1] I. Veronese, C. De Mattia, M. Fasoli, N. Chiodini, E. Mones, M. C. Cantone, and A. Vedda, "Infrared luminescence for real time ionizing radiation detection," Appl. Phys. Lett. **105**, 061103 (2014).

[2] N. Savard, D. Potkins, J. Beaudry, A. Jirasek, C. Duzenli, and C. Hoehr, "Characteristics of a Ce-doped silica fiber irradiated by 74 MeV protons," Radiat. Meas. **114**, 19–24 (2018).

[3] P. Lecoq, "New crystal technologies for novel calorimeter concepts," J. Phys. Conf. Ser. **160**, 012016 (2009).

[4] C. Dujardin, C. Mancini, D. Amans, G. Ledoux, D. Abler, E. Auffray, P. Lecoq, D. Perrodin, A. Petrosyan, and K. L. Ovanesyan, "LuAG:Ce fibers for high energy calorimetry," J. Appl. Phys. **108**, 013510 (2010).

[5] M. Lucchini, T. Medvedeva, K. Pauwels, C. Tully, A. Heering, C. Dujardin, K. Lebbou, P. Lecoq, and E. Auffray, "Test beam results with LuAG fibers for next-generation calorimeters," J. Instrum. **8**, P10017–P10017 (2013).

[6] A. Benaglia, M. Lucchini, K. Pauwels, C. Tully, T. Medvedeva, A. Heering, C. Dujardin, V. Kononets, K. Lebbou, N. Aubry, S. Faraj, G. Ferro, P. Lecoq, and E. Auffray, "Test beam results of a high granularity LuAG fibre calorimeter prototype," J. Instrum. **11**, P05004–P05004 (2016).

[7] K. Pauwels, M. Lucchini, A. Benaglia, and E. Auffray, "Calorimeter designs based on fibre-shaped scintillators," in *Engineering of Scintillation Materials and Radiation Technologies*, edited by M. Korzhik and A. Gektin (Springer International Publishing, Cham, 2017) pp. 231–241.

[8] R. Becker, G. Dissertori, A. Gendotti, Q. Huang, D. Luckey, W. Lustermann, S. Lutterer, F. Nessi-Tedaldi, F. Pandolfi, and F. Pauss, "Proof-of-principle of a new geometry for sampling calorimetry using inorganic scintillator plates," J. Phys. Conf. Ser. **587**, 012039 (2015).

[9] D. Contardo, M. Klute, J. Mans, L. Silvestris, and J. Butler, *Technical Proposal for the Phase-II Upgrade of the CMS detector*, Tech. Rep. CERN-LHCC-2015-010. LHCC-P-008. CMS-TDR-15-02 (CERN, Geneva, 2015).

[10] S. Lee, M. Livan, and R. Wigmans, "Dual-Readout Calorimetry," Rev. Mod. Phys. (2017), http://arxiv.org/abs/1712.05494v1.

[11] N. Akchurin, O. Atramentov, K. Carrell, K. Z. Gümüş, J. Hauptman, H. Kim, H. P. Paar, A. Penzo, and R. Wigmans, "Separation of scintillation and Cherenkov light in an optical calorimeter," Nucl. Instrum. Methods Phys. Res. A **550**, 185 – 200 (2005).

[12] E. Auffray, D. Abler, P. Lecoq, and G. Mavromanolakis, "Dual Readout with PWO Crystals and LuAG Crystal Scintillating Fibers," IEEE Trans. Nucl. Sci. **57**, 1454–1459 (2010).

[13] N. Akchurin, F. Bedeschi, A. Cardini, M. Cascella, G. Ciapetti, A. d'Orazio, L. Collica, D. De Pedis, R. Ferrari, S. Franchino, M. Fraternali, G. Gaudio, P. Genova, J. Hauptman, F. Lacava, L. La Rotonda, S. Lee, M. Livan, E. Meoni, A. Negri, D. Pinci, A. Policicchio, F. Scuri, A. Sill, T. Venturelli, C. Voena, and R. Wigmans, "Detection of electron showers in dual-readout crystal calorimeters," Nucl. Instrum. Methods Phys. Res. A **686**, 125 – 135 (2012).

[14] W. J. Yoo, S. H. Shin, D. Jeon, S. Hong, S. G. Kim, H. I. Sim, K. W. Jang, S. Cho, and B. Lee, "Simultaneous measurements of pure scintillation and Cerenkov signals in an integrated fiber-optic dosimeter for electron beam therapy dosimetry," Opt. Express **21**, 27770 (2013).

[15] T. M. Shaffer, C. M. Drain, and J. Grimm, "Optical Imaging of Ionizing Radiation from Clinical Sources," J. Nuc. Med. **57**, 1661–1666 (2016).

[16] A. Arodzero, S. Boucher, J. Hartzell, S. V. Kutsaev, R. C. Lanza, V. Palermo, S. Vinogradov, and V. Ziskin, "High speed, low dose, intelligent X-ray cargo inspection," in *Proc. IEEE Nucl. Sci. Symp. and Med. Imaging Conf. (NSS/MIC)* (2015) pp. 1–7.

[17] A. Arodzero, "Scintillation-Cherenkov detectors and method for high energy x-ray cargo container imaging and industrial radiography," (2011).

[18] M. Christl, J. H. Adams Jr, E. N. Kuznetsov, and S. Nazzel, "A Solar and Energetic Particle and Spectrometer (SEPS) and Concept," in *PROC. OF THE 31st ICRC* (2009).

[19] M. T. Lucchini, K. Pauwels, K. Blavzek, S. Ochesanu, and E. Auffray, "Radiation Tolerance of LuAG:Ce and YAG:Ce Crystals under High Levels of Gamma- and Proton-Irradiation," IEEE Trans. Nucl. Sci. **63**, 586–590 (2016).

[20] B. J. Singleton, B. S. Jones, A. A. Bickley, J. C. Petrosky, J. W. McClory, and B. R. Kowash, "Radiation effects on YAG:Ce scintillating fiber," in *IEEE Nucl. Sci. Symp. Conf. Record* (2011) pp. 1935–1940.

[21] K. Pauwels, C. Dujardin, S. Gundacker, K. Lebbou, P. Lecoq, M. Lucchini, F. Moretti, A. G. Petrosyan, X. Xu, and E. Auffray, "Single crystalline LuAG fibers for homogeneous dual-readout calorimeters," J. Instrum. **8**, P09019–P09019 (2013).

[22] V. Kononets, E. Auffray, C. Dujardin, S. Gridin, F. Moretti, G. Patton, K. Pauwels, O. Sidletskiy, X. Xu, and K. Lebbou, "Growth of long undoped and Ce-doped LuAG single crystal fibers for dual readout calorimetry," J. Cryst. Growth **435**, 31 – 36 (2016).

[23] A. E. Dosovitskiy, G. A. Dosovitskiy, and M. V. Korjik, "Development of the new generation of glass-based neutron detection materials," PROC. SPIE (2012), 10.1117/12.946595.

[24] Z. Kang, B. K. Wagner, C. J. Summers, J. Nadler, R. Rosson, and B. Kahn, "Polymer and glass-matrix nanocomposites for scintillation applications," in *IEEE Nucl. Sci. Symp. and Med. Imaging Conf. (NSS/MIC)* (2012) pp. 1688–1691.

[25] T. Yanagida, J. Ueda, H. Masai, Y. Fujimoto, and S. Tanabe, "Optical and scintillation properties of Ce-doped $34Li_2O$–$5MgO$–$10Al_2O_3$–$51SiO_2$ glass," J. Non-Cryst. Solids **431**, 140 – 144 (2016).

[26] N. Akchurin, C. Cowden, J. Damgov, C. Dragoiu, P. Dudero, J. Faulkner, and S. Kunori, "Cerium-doped scintillating fused-silica fibers," J. Instrum. **13**, P04010 (2018).

[27] A. Vedda, N. Chiodini, D. Di Martino, M. Fasoli, S. Keffer, A. Lauria, M. Martini, F. Moretti, and G. Spinolo, "Ce^{3+}-doped fibers for remote radiation dosimetry," Appl. Phys. Lett. **85**, 6356–6358 (2004).

[28] A. Vedda, N. Chiodini, D. Di Martino, M. Fasoli, F. Morazzoni, F. Moretti, R. Scotti, G. Spinolo, A. Baraldi, R. Capelletti, M. Mazzera, and M. Nikl, "Insights into Microstructural Features Governing Ce^{3+} Luminescence Efficiency in Sol-Gel Silica Glasses," Chem. Mater. **18**, 6178–6185 (2006), https://doi.org/10.1021/cm0617541.

[29] A. Penzo, Y. Onel, and the CMS Collaboration, "The CMS-HF quartz fiber calorimeters," J. Phys.: Conf. Ser. **160**, 012014 (2009).

[30] F. Cova, M. Fasoli, F. Moretti, N. Chiodini, K. Pauwels, E. Auffray, M. T. Lucchini, E. Bourret, I. Veronese, E. d'Ippolito, and A. Vedda, "Optical properties and radiation hardness of Pr-doped sol-gel silica: Influence of fiber drawing process," J. Lumin. **192**, 661 – 667 (2017).

[31] F. Cova, F. Moretti, M. Fasoli, N. Chiodini, K. Pauwels, E. Auffray, M. T. Lucchini, S. Baccaro, A. Cemmi, H. Bártová, and A. Vedda, "Radiation hardness of Ce-doped sol-gel silica fibers for high energy physics applications," Opt. Lett. **43**, 903 (2018).

[32] P. A. Rodnyi, *Physical processes in inorganic scintillators*, Vol. 14 (CRC press, 1997).

[33] J. Spanggaard, *Delay Wire Chambers - A Users Guide*, Tech. Rep. SL-Note-98-023-BI (CERN, Geneva, 1998).

[34] A. N. Vasil'ev, "Microtheory of scintillation in crystalline materials," in *International Conference on Engineering of Scintillation Materials and Radiation Technologies* (Springer, 2016) pp. 3–34.

[35] C. Grupen and B. Shwartz, *Particle detectors* (Cambridge University Press, 2008).

[36] P. Križan, "Recent progress in particle identification methods," Nucl. Instrum. Methods Phys. Res. A **598**, 130 – 137 (2009).

[37] J. P. Hayward, C. L. Hobbs, Z. W. Bell, L. A. Boatner, R. E. Johnson, J. O. Ramey, G. E. Jellison, and C. R. Lillard, "Characterizing the radiation response of Cherenkov glass detectors with isotopic sources," J. Radioanal. Nucl. Chem. **295**, 1143–1151 (2013).

[38] C. W. Fabjan and F. Gianotti, "Calorimetry for particle physics," Rev. Mod. Phys. **75**, 1243–1286 (2003).

[39] M. T. Lucchini, E. Auffray, A. Benaglia, F. Cavallari, D. Cockerill, A. Dolgopolov, J. L. Faure, N. Golubev, P. R. Hobson, S. Jain, M. Korjik, V. Mechinski, A. Singovski, T. Tabarelli de Fatis, I. Tarasov, and S. Zahid, "Double side read-out technique for mitigation of radiation damage effects in $PbWO_4$ crystals," J. Instrum. **11**, P04021–P04021 (2016).